Delay and Doppler spreads in underwater acoustic particle velocity channels

Huaihai Guo[a)] and Ali Abdi
Center for Wireless Communication and Signal Processing Research, Department of Electrical and Computer Engineering, New Jersey Institute of Technology, Newark, New Jersey 07102

Aijun Song and Mohsen Badiey
Physical Ocean Science and Engineering, College of Earth, Ocean, and Environment, University of Delaware, Newark, Delaware 19716

(Received 24 March 2010; revised 9 December 2010; accepted 10 December 2010)

Signal processing and communication in acoustic particle velocity channels using vector sensors are of interest in the underwater medium. Due to the presence of multiple propagation paths, a mobile receiver collects the signal with different delays and Doppler shifts. This introduces certain delay and Doppler spreads in particle velocity channels. In this paper, these channel spreads are characterized using the zero-crossing rates of channel responses in frequency and time domain. Useful expressions for delay and Doppler spreads are derived in terms of the key channel parameters mean angle of arrival and angle spread. These results are needed for design and performance prediction of systems that utilize underwater acoustic particle velocity and pressure channels.
 [DOI: 10.1121/1.3533721]

PACS number(s): 43.60.Cg, 43.60.Dh [NPC] Pages: 2015–2025

I. INTRODUCTION

Data communication is of interest in numerous naval and civilian applications. Examples include communication among autonomous underwater vehicles (AUVs) for collaborative operations, harbor security systems, tactical surveillance applications, oceanographic data retrieval from underwater sensors over geographically large areas, offshore oil and gas explorations, etc. After the first generation of analog modems, second generation digital modems in 80's used noncoherent techniques such as frequency shift keying and differentially coherent schemes like differential phase shift keying (DPSK).[1] Due to the need for higher spectral efficiencies, coherent systems with phase shift keying and quadrature amplitude modulation were developed in 90's.[2,3] Spatial diversity with arrays of hydrophones and different types of equalization, beamforming, coding, channel estimation, and tracking are also used for underwater communication.[1] Underwater multiple-input multiple-output (MIMO) systems using spatially separated pressure sensors are also recently investigated.[4–7]

A vector sensor can measure non-scalar components of the acoustic field such as the particle velocity, which cannot be sensed by a single scalar (pressure) sensor. Development of vector sensors dates back to 30's.[8] In the past few decades, a large volume of research has been conducted on theory, performance evaluation, and design of vector sensors. They have been mainly used for target localization and sound navigation and ranging (SONAR) applications. Examples include accurate beamforming and azimuth/elevation estimation of a source, avoiding the left–right ambiguity of linear towed arrays of scalar sensors, significant acoustic noise reduction due to the highly directive beam pattern, etc.[9–12]

Vector sensors have recently been proposed[13,14] and then used[15,16] for underwater acoustic communication. Characterization of particle velocity channels and their impact on vector sensor communication systems performance is therefore of interest. In multipath channels such as shallow waters, a vector sensor receives the signal through several paths and each path has a different delay (travel time). Motion of the transmitter or receiver in a multipath channel introduces different Doppler shifts as well. The largest differences between the path delays and between the Doppler shifts are called delay spread and Doppler spread, respectively.[17] The harsh multipath, with delay spreads up to hundreds of symbols for high data rates, and temporal variations of the underwater acoustic channels, with Doppler spreads up to several tens of hertz, are major issues in underwater acoustic communication.[1] Some typical values for delay spread[18,19] and Doppler spread[20,21] of the underwater acoustic channel are 5–15 ms and 6–30 Hz, respectively. Knowledge of delay and Doppler spreads in acoustic particle velocity channels is important for efficient design of underwater vector sensor communication systems. Characterization of delay and Doppler spreads in terms of the physical parameters of the propagation environment is needed for system performance prediction as well.

In general, the zero-crossing rate (ZCR) of a random process carries useful information that can be used for various purposes. Examples include signal detection,[22] estimation of the density of scatterers,[23] calculating sonar false alarm probability,[24] characterization of acoustic emission signals,[25] speech recognition,[26] etc.

It is also well known that delay and Doppler spreads are proportional to the ZCRs of the channel in frequency[27,28] and time[29,30] domains, respectively. In Fig. 1 the physical meaning of frequency-domain ZCR and its connection with

[a)]Author to whom correspondence should be addressed: Electronic mail: hg45@njit.edu

delay spread are shown. Let the Fourier pair $P(f)$ and $p(\tau)$ represent the complex channel transfer function and impulse response, respectively, where f and τ are frequency and time delay in hertz and seconds, respectively. As shown in Fig. 1(a), $\mathrm{Re}\{P(f)\}$ slowly varies with f, where $\mathrm{Re}\{.\}$ gives the real part. This slow variation results in a small number of times that the channel transfer function crosses the zero level, i.e., low ZCR. In this figure there are nine zero crossings over 10 Hz, which gives a ZCR of 0.9. The magnitude of the channel impulse response, $|p(\tau)|$, is shown in Fig. 1(b), which has a relatively small delay spread. This is because of the well-known inverse relationship between frequency-axis and time-axis scalings, i.e., waveform expansion in one domain results in compression in the other domain. On the other hand, when the ZCR of the channel transfer function is higher, as shown in Fig. 1(c), one can say the channel transfer function is compressed in the f domain. This results in the expansion of the channel impulse response in the τ domain shown in Fig. 1(d), which now has a larger delay spread. The connection between time-domain ZCR and Doppler spread can be similarly explained.

To calculate the frequency- and time-domain ZCRs, one needs to obtain the second derivative of the corresponding frequency and temporal channel correlations, respectively, as explained in Sec. IV. Therefore, to calculate delay and Doppler spreads in particle velocity channels, expressions for frequency and temporal correlations of such channels should be derived first.

In what follows, basic formulas and definitions for particle velocity channels are provided in Sec. II A statistical model for particle velocity channels sensed by a moving vector sensor array is developed in Sec. III and channel correlation functions are derived as well. Using the frequency and temporal correlation functions, frequency- and time-domain ZCRs are calculated in Sec. IV for both pressure and particle velocity channels. Numerical results and concluding remarks are provided in Secs. V and VI, respectively.

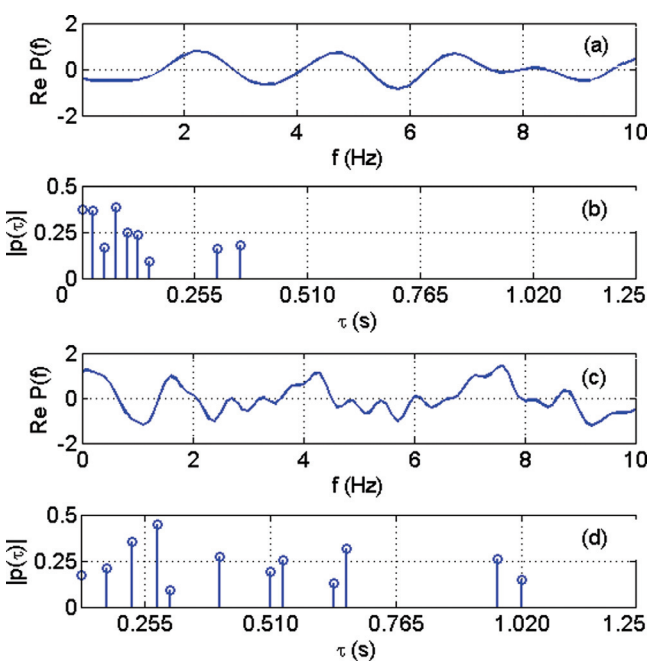

FIG. 1. (Color online) Graphical representation of the connection between the ZCR of a channel transfer function and the delay spread of the corresponding channel impulse response: (a) A channel transfer function with low ZCR, (b) the corresponding channel impulse response with small delay spread, (c) a channel transfer function with high ZCR, and (d) the corresponding channel impulse response with large delay spread.

II. DEFINITIONS OF PARTICLE VELOCITY CHANNELS

As an underwater acoustic communication receiver, we consider the vector sensor array shown in Fig. 2, in the two-dimensional y–z (range-depth) plane. There is one pressure sensor transmitter in the far field, called Tx, shown by a black circle. We have three receive vector sensors Rx, Rx_1, and Rx_2, represented by black squares, with the center of array located at $y=0$ and $z=D$. Each vector sensor measures the pressure, as well as the y and z components of the acoustic particle velocity, all in a single co-located point. This means there are three pressure channels p, p_1, and p_2, as well as six *pressure-equivalent* velocity channels p^y, p^z, p_1^y, p_1^z, p_2^y, and p_2^z, all measured in Pascal (Newton/m^2). In Fig. 2 pressure channels are represented by solid straight lines, whereas the y-velocity channels and the z-velocity channels are represented by dashed curved lines and dotted curved lines, respectively. The particle velocity channels v^y, v^z, v_1^y, v_1^z, v_2^y, and v_2^z are defined as

$$v^y = -\frac{1}{j\rho_0\omega_0}\frac{\partial p}{\partial y}, \quad v^z = -\frac{1}{j\rho_0\omega_0}\frac{\partial p}{\partial z},$$
$$v_1^y = -\frac{1}{j\rho_0\omega_0}\frac{\partial p_1}{\partial y}, \quad v_1^z = -\frac{1}{j\rho_0\omega_0}\frac{\partial p_1}{\partial z},$$
$$v_2^y = -\frac{1}{j\rho_0\omega_0}\frac{\partial p_2}{\partial y}, \quad v_2^z = -\frac{1}{j\rho_0\omega_0}\frac{\partial p_2}{\partial z}. \tag{1}$$

In the above equations ρ_0 is the density of the fluid in kg/m^3, $j^2=-1$ and $\omega_0=2\pi f_0$ is the frequency in rad/s. By multiplying the velocity channels in Eq. (1) with $-\rho_0 c$, the negative of the acoustic impedance of the fluid, where c is the sound speed in m/s, we obtain the pressure-equivalent velocity

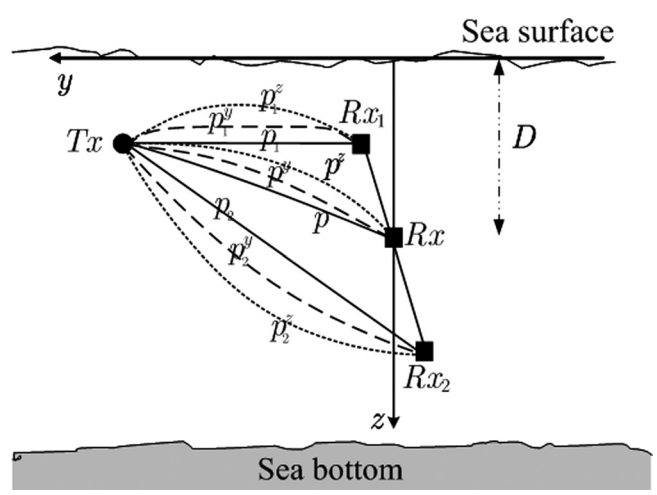

FIG. 2. A system with one pressure transmitter and three vector sensor receivers. Each vector sensor measures the pressure, and the y and z components of the acoustic particle velocity.

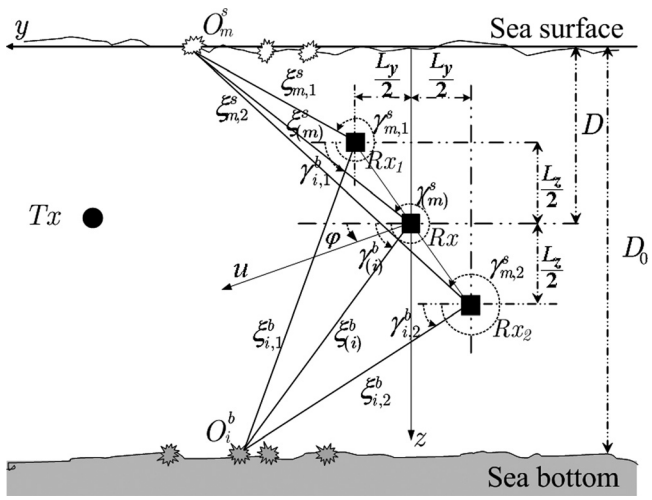

FIG. 3. Received rays at the three vector sensors in a multipath shallow water channel.

channels p^y, p^z, p_1^y, p_1^z, p_2^y, and p_2^z. Note that $p^y = -\rho_0 c v^y$, $p^z = -\rho_0 c v^z$, $p_1^y = -\rho_0 c v_1^y$, $p_1^z = -\rho_0 c v_1^z$, $p_2^y = -\rho_0 c v_2^y$, and $p_2^z = -\rho_0 c v_2^z$. With λ as the wavelength in m and $k = 2\pi/\lambda = \omega_0/c$ as the wavenumber in rad/m, finally we obtain,

$$p^y = \frac{1}{jk}\frac{\partial p}{\partial y}, \quad p^z = \frac{1}{jk}\frac{\partial p}{\partial z},$$
$$p_1^y = \frac{1}{jk}\frac{\partial p_1}{\partial y}, \quad p_1^z = \frac{1}{jk}\frac{\partial p_1}{\partial z},$$
$$p_2^y = \frac{1}{jk}\frac{\partial p_2}{\partial y}, \quad p_2^z = \frac{1}{jk}\frac{\partial p_2}{\partial z}. \tag{2}$$

The received rays at the vector sensor array are shown in Fig. 3 where D_0 is the water depth. Vector sensor 1 is located at $y = L_y/2$ and $z = D - (L_z/2)$, vector sensor 2 is at $y = -L_y/2$ and $z = D + (L_z/2)$ and vector sensor Rx is located at $y = 0$ and $z = D$. Here, L_y and L_z are the projections of the array length L at y and z axis, respectively, such that $L = (L_y^2 + L_z^2)^{1/2}$. All the angles are measured with respect to the positive direction of y, counterclockwise. We model the rough sea bottom and its surface as collections of N^b and N^s scatterers, respectively, such that $N^b \gg 1$ and $N^s \gg 1$. In this paper, the small letters b and s refer to the bottom and surface, respectively. In Fig. 3, for example, the i-th bottom scatterer is represented by O_i^b, $i = 1, 2, \ldots, N^b$, whereas O_m^s denotes the m-th surface scatterer, $m = 1, 2, \ldots, N^s$. Rays scattered from the bottom and the surface toward the vector sensors are shown by solid lines. The rays scattered from O_i^b hit Rx_1 and Rx_2 at the angle of arrivals (AOAs) $\gamma_{i,1}^b$ and $\gamma_{i,2}^b$, respectively. The traveled distances are labeled by $\xi_{i,1}^b$ and $\xi_{i,2}^b$, respectively. Similarly, the scattered rays from O_m^s impinge Rx_1 and Rx_2 at the AOAs $\gamma_{m,1}^s$ and $\gamma_{m,2}^s$, respectively, with $\xi_{m,1}^s$ and $\xi_{m,2}^s$ as the traveled distances shown in Fig. 3. The vector sensor receivers move at the speed u, in the direction specified by φ in Fig. 3.

III. CHANNEL CORRELATION FUNCTIONS

In a multipath channel, delay spread and Doppler spread are key channel characteristics for system design. As discussed previously, delay and Doppler spreads are represented by frequency- and time-domain ZCRs of the channel, respectively. Furthermore, frequency- and time-domain ZCRs are related to the second derivative of frequency and temporal channel correlations, respectively. To obtain these channel correlation functions, in what follows we consider a statistical framework that leads us to frequency-time-space correlation functions for particle velocity channels. By taking proper derivatives of these correlation functions, ZCRs of interest will be obtained.

Superposition of plane waves at the mobile sensors Rx_1 and Rx_2 results in the following time-varying transfer functions $P_1(f, t)$ and $P_2(f, t)$ for the pressure channels,

$$\begin{aligned} P_1(f,t) =& (\Lambda_b/N^b)^{1/2} \sum_{i=1}^{N^b} \{a_i^b \exp(j\psi_i^b) \\ & \times \exp(jk[y\cos(\gamma_{i,1}^b) + z\sin(\gamma_{i,1}^b)]) \\ & \times \exp(-j2\pi f \tau_{i,1}^b) \\ & \times \exp(j2\pi f_M \cos(\gamma_{i,1}^b - \varphi)t)\}\Big|_{\substack{y=L_y/2,\\ z=D-L_z/2}} \\ & + ((1-\Lambda_b)/N^s)^{1/2} \sum_{m=1}^{N^s} \{a_m^s \exp(j\psi_m^s) \\ & \times \exp(jk\,[y\cos(\gamma_{m,1}^s) + z\sin(\gamma_{m,1}^s)]) \\ & \times \exp(-j2\pi f \tau_{m,1}^s) \\ & \times \exp(j2\pi f_M \cos(\gamma_{m,1}^s - \varphi)t)\}\Big|_{\substack{y=L_y/2,\\ z=D-L_z/2}}, \end{aligned} \tag{3}$$

$$\begin{aligned} P_2(f,t) =& (\Lambda_b/N^b)^{1/2} \sum_{i=1}^{N^b} \{a_i^b \exp(j\psi_i^b) \\ & \times \exp(jk[y\cos(\gamma_{i,2}^b) + z\sin(\gamma_{i,2}^b)]) \\ & \times \exp(-j2\pi f \tau_{i,2}^b) \\ & \times \exp(j2\pi f_M \cos(\gamma_{i,2}^b - \varphi)t)\}\Big|_{\substack{y=-L_y/2,\\ z=D+L_z/2}} \\ & + ((1-\Lambda_b)/N^s)^{1/2} \sum_{m=1}^{N^s} \{a_m^s \exp(j\psi_m^s) \\ & \times \exp(jk[y\cos(\gamma_{m,2}^s) + z\sin(\gamma_{m,2}^s)]) \\ & \times \exp(-j2\pi f \tau_{m,2}^s) \\ & \times \exp(j2\pi f_M \cos(\gamma_{m,2}^s - \varphi)t)\}\Big|_{\substack{y=-L_y/2,\\ z=D+L_z/2}}. \end{aligned} \tag{4}$$

Note that $P_1(f, t)$ in Eq. (3) is the sum of two summations, one multiplied by $(\Lambda_b/N^b)^{1/2}$ and the other one by $((1-\Lambda_b)/N^b)^{1/2}$. The first summation has N^b terms, and each term is the product of a_i^b and four complex exponentials $\exp(j\psi_i^b)$, $\exp(jk\,[y\cos(\gamma_{i,1}^b) + z\sin(\gamma_{i,1}^b)])$, $\exp(-j2\pi f \tau_{i,1}^b)$ and $\exp(j2\pi f_M \cos(\gamma_{i,1}^b - \varphi)t)$. The second summation in Eq. (3) has N^s terms, and each term is the product of a_m^s and

four other complex exponentials. Similar explanations hold for $P_2(f, t)$ and its two summations in Eq. (4). In Eqs. (3) and (4), $a_i^b > 0$ and $a_m^s > 0$ represent the amplitudes of the rays scattered from O_i^b and O_m^s, respectively, whereas $\psi_i^b \in [0, 2\pi)$ and $\psi_m^s \in [0, 2\pi)$ stand for the associated phases. The delays τ in Eqs. (3) and (4) represent the travel times from the bottom and surface scatterers to the two vector sensors. For example, $\tau_{i,1}^b$ denotes the travel time from O_i^b to Rx_1. Moreover, the AOAs γ in Eqs. (3) and (4) stand for the propagation directions of waves scattered from the bottom and surface toward the receivers. For instance, $\gamma_{m,2}^s$ is the AOA of a ray at Rx_2 which is coming from O_m^s. The complex exponential of the form $\exp(jk[y \cos(\gamma) + z \sin(\gamma)])$ in Eqs. (3) and (4) represent a plane wave with the AOA γ at the point (y, z), $\exp(-j2\pi f\tau)$ specifies that the plane wave's travel time is τ,[31] and $\exp(j2\pi f_M \cos(\gamma - \varphi)t)$ corresponds to its Doppler shift introduced by the motion of the receiver.[32,33] Here $f_M = u/\lambda$ is the maximum Doppler shift. The terms $(N^b)^{-1/2}$ and $(N^s)^{-1/2}$ are included in Eqs. (3) and (4) to scale the power. Moreover, $0 \le \Lambda_b \le 1$ represents the amount of the contribution of the bottom scatterers, whereas the contribution of the surface scatterers is given by $1 - \Lambda_b$.

Based on the definition of the correlation function $CP_2P_1(\Lambda f, \Lambda t, L_z, L_y) = E[P_2(f + \Delta f, t + \Delta t)P_1^*(f, t)]$ and the channel representations in Eqs. (3) and (4), an integral expression can be similarly[31,34] obtained for the frequency-time-space pressure channel correlation,

$$C_{P_2P_1}(\Delta f, \Delta t, L_z, L_y) = \Lambda_b \int_{\gamma^b=0}^{\pi} \left\{ \begin{array}{l} w^b(\gamma^b) \exp[-jkL_y(\cos(\gamma_2^b) + \cos(\gamma_1^b))/2] \exp[jkD(\sin(\gamma_2^b) - \sin(\gamma_1^b))] \\ \times \exp[jkL_z(\sin(\gamma_2^b) + \sin(\gamma_1^b))/2] \exp[j2\pi f(\tau_1^b - \tau_2^b)] \\ \times \exp[-j2\pi\Delta f \tau_2^b] \exp[j2\pi f_M \cos(\gamma^b - \varphi)\Delta t] \end{array} \right\} d\gamma^b$$
$$+ (1 - \Lambda_b) \int_{\gamma^s=\pi}^{2\pi} \left\{ \begin{array}{l} w^s(\gamma^s) \exp[-jkL_y(\cos(\gamma_2^s) + \cos(\gamma_1^s))/2] \exp[jkD(\sin(\gamma_2^s) - \sin(\gamma_1^s))] \\ \times \exp[jkL_z(\sin(\gamma_2^s) + \sin(\gamma_1^s))/2] \exp[j2\pi f(\tau_1^s - \tau_2^s)] \\ \times \exp[-j2\pi\Delta f \tau_2^s] \exp[j2\pi f_M \cos(\gamma^s - \varphi)\Delta t] \end{array} \right\} d\gamma^s. \quad (5)$$

Each integrand in Eq. (5) is the product of a w function defined later, and six complex exponentials. Note that γ^b and γ^s are the AOAs of rays coming from bottom and surface toward the array center, respectively. The terms $\cos(\gamma_q^b)$, $\cos(\gamma_q^s)$, $\sin(\gamma_q^b)$ and $\sin(\gamma_q^s)$, $q = 1, 2$, represent the corresponding cosine and sine of bottom and surface AOAs for the vector sensors Rx_1 and Rx_2, respectively. Moreover, τ_q^b and τ_q^s, $q = 1, 2$ are travel times from the bottom and surface scatterers to Rx_1 and Rx_2, respectively. As shown in Appendix A, all these parameters can be written in terms of D, D_0, γ^b, γ^s, L_z, and L_y. Finally, $w^b(\gamma^b)$ and $w^s(\gamma^s)$ in Eq. (5) are the probability density functions (PDFs) of the AOAs of the waves coming from the sea bottom and surface, respectively, such that $0 < \gamma^b < \pi$ and $\pi < \gamma^s < 2\pi$.

Similarly,[31] to obtain pressure–velocity and velocity–velocity channel correlations, one need to take proper derivatives of the pressure channel correlation in Eq. (5), as summarized below:

$$C_{P_2P_1^z}(\Delta f, \Delta t, L_z, L_y) = E[P_2(f + \Delta f, t + \Delta t)\{P_1^z(f, t)\}^*] = (jk)^{-1}\partial C_{P_2P_1}(\Delta f, \Delta t, L_z, L_y)/\partial L_z, \quad (6)$$

$$C_{P_2P_1^y}(\Delta f, \Delta t, L_z, L_y) = E[P_2(f + \Delta f, t + \Delta t)\{P_1^y(f, t)\}^*] = (jk)^{-1}\partial C_{P_2P_1}(\Delta f, \Delta t, L_z, L_y)/\partial L_y, \quad (7)$$

$$C_{P_2^zP_1^z}(\Delta f, \Delta t, L_z, L_y) = E[P_2^z(f + \Delta f, t + \Delta t)\{P_1^z(f, t)\}^*] = -k^{-2}\partial^2 C_{P_2P_1}(\Delta f, \Delta t, L_z, L_y)/\partial L_z^2, \quad (8)$$

$$C_{P_2^yP_1^y}(\Delta f, \Delta t, L_z, L_y) = E[P_2^y(f + \Delta f, t + \Delta t)\{P_1^y(f, t)\}^*] = -k^{-2}\partial^2 C_{P_2P_1}(\Delta f, \Delta t, L_z, L_y)/\partial L_y^2, \quad (9)$$

$$C_{P_2^zP_1^y}(\Delta f, \Delta t, L_z, L_y) = E[P_2^z(f + \Delta f, t + \Delta t)\{P_1^y(f, t)\}^*] = -k^{-2}\partial^2 C_{P_2P_1}(\Delta f, \Delta t, L_z, L_y), /\partial L_z \partial L_y. \quad (10)$$

In Eqs. (6)–(10), the time-varying transfer functions for the pressure-equivalent velocity channels at the q-th vector sensor, $q = 1, 2$, are defined as $P_q^z(f, t) = (jk)^{-1}\partial P_q(f, t)/\partial z$ and $P_q^y(f, t) = (jk)^{-1}\partial P_q(f, t)/\partial y$.

Now, we focus on the vector sensor receiver Rx, to calculate the delay and Doppler spreads of particle velocity channels. With $L_z = L_y = 0$ in Eq. (5), it is straight forward to obtain the frequency-time autocorrelation of $P(f, t)$, the time-varying transfer function of the pressure channel, at Rx,

$$\begin{aligned} C_{PP}(\Delta f, \Delta t) &= E[P(f + \Delta f, t + \Delta t)P^*(f, t)] \\ &= C_{P_2P_1}(\Delta f, \Delta t, 0, 0) \\ &= \Lambda_b E_{\gamma^b}[\exp[-j2\pi\Delta f T_b/\sin(\gamma^b)] \\ &\quad \times \exp[j2\pi f_M \cos(\gamma^b - \varphi)\Delta t]] \\ &\quad + (1 - \Lambda_b)E_{\gamma^s}[\exp[-j2\pi\Delta f T_s/\sin(\gamma^s)] \\ &\quad \times \exp[j2\pi f_M \cos(\gamma^s - \varphi)\Delta t]]. \end{aligned} \quad (11)$$

Here $T_b = (D_0 - D)/c$, the vertical travel time from bottom to Rx and $T_s = D/c$, the vertical travel time from surface to

Rx. Equation (11) is obtained because when $L_z = L_y = 0$, Eqs. (A1)–(A9) in Appendix A result in $\gamma_2^b = \gamma_1^b$, $\tau_2^b = \tau_1^b$, $\tau_2^b = T_b/\sin(\gamma^b)$, $\gamma_2^s = \gamma_1^s$, $\tau_2^s = \tau_1^s$, and $\tau_2^s = T_s/\sin(\gamma^s)$. Let us define the time-varying transfer functions for the pressure-equivalent velocity channels at the vector sensor Rx as $P^z(f, t) = (jk)^{-1}\ \partial P(f, t)/\partial z$ and $P^y(f, t) = (jk)^{-1}\partial P(f, t)/\partial y$. Then using Eqs. (8) and (9), the second derivative of Eq. (5) at $L_z = L_y = 0$ provide the following frequency-time autocorrelations of $P^z(f, t)$ and $P_y(f, t)$ at Rx, respectively.

$$\begin{aligned} C_{P^zP^z}(\Delta f, \Delta t) &= E[P^z(f+\Delta f, t+\Delta t)\{P^z(f,t)\}^*] \\ &= C_{P_2^zP_1^z}(\Delta f, \Delta t, 0, 0) \\ &= \Lambda_b E_{\gamma^b}\left[\sin^2(\gamma^b)\exp[-j2\pi\Delta f T_b/\sin(\gamma^b)]\right. \\ &\quad \times \exp[j2\pi f_M \cos(\gamma^b - \varphi)\Delta t]\Big] \\ &\quad +(1-\Lambda_b)E_{\gamma^s}\left[\sin^2(\gamma^s)\right. \\ &\quad \times \exp[-j2\pi\Delta f T_s/\sin(\gamma^s)] \\ &\quad \times \exp[j2\pi f_M \cos(\gamma^s - \varphi)\Delta t]\Big], \end{aligned} \tag{12}$$

$$\begin{aligned} C_{P^yP^y}(\Delta f, \Delta t) &= E[P^y(f+\Delta f, t+\Delta t)\{P^y(f,t)\}^*] \\ &= C_{P_2^yP_1^y}(\Delta f, \Delta t, 0, 0) \\ &= \Lambda_b E_{\gamma^b}\left[\cos^2(\gamma^b)\exp[-j2\pi\Delta f T_b/\sin(\gamma^b)]\right. \\ &\quad \times \exp[j2\pi f_M \cos(\gamma^b - \varphi)\Delta t]\Big] \\ &\quad +(1-\Lambda_b)E_{\gamma^s}\left[\cos^2(\gamma^s)\right. \\ &\quad \times \exp[-j2\pi\Delta f T_s/\sin(\gamma^s)] \\ &\quad \times \exp[j2\pi f_M \cos(\gamma^s - \varphi)\Delta t]\Big]. \end{aligned} \tag{13}$$

Before concluding this section, we derived the correlation between the real parts of $P_1(f, t)$ and $P_2(f, t)$ in Eqs. (3) and (4). This will be needed to compute the ZCR of real channel functions in the next section. If W is complex, then $Re\{W\} = (W + W^*)/2$. This results in

$$\begin{aligned} &E[\mathrm{Re}\{P_2(f+\Delta f, t+\Delta t)\}\mathrm{Re}\{P_1(f,t)\}] \\ &= \frac{1}{2}\mathrm{Re}\{C_{P_2P_1}(\Delta f, \Delta t, L_z, L_y)\} \\ &\quad + \frac{1}{2}\mathrm{Re}\{E[P_2(f+\Delta f, t+\Delta t)P_1(f,t)]\}, \end{aligned} \tag{14}$$

where $C_{P_2P_1}(\Delta f, \Delta t, L_z, L_y)$ is given in Eq. (5). Based on the statistical properties of phases ψ_i^b and ψ_m^s, independent and uniformly distributed over 2π radians, it can be verified that the second term on the right hand side of Eq. (14) is zero. This yields

$$\begin{aligned} &E[\mathrm{Re}\{P_2(f+\Delta f, t+\Delta t)\}\mathrm{Re}\{P_1(f,t)\}] \\ &= \frac{1}{2}\mathrm{Re}\{C_{P_2P_1}(\Delta f, \Delta t, L_z, L_y)\}. \end{aligned} \tag{15}$$

Similarly, based on the definitions of $P_q^z(f,t)$ and $P_q^y(f,t)$, $q = 1, 2$, provided after Eq. (10), we obtain,

$$\begin{aligned} &E\left[\mathrm{Re}\left\{P_2^z(f+\Delta f, t+\Delta t)\right\}\mathrm{Re}\left\{P_1^z(f,t)\right\}\right] \\ &= \frac{1}{2}\mathrm{Re}\left\{C_{P_2^zP_1^z}(\Delta f, \Delta t, L_z, L_y)\right\}, \end{aligned} \tag{16}$$

$$\begin{aligned} &E\left[\mathrm{Re}\left\{P_2^y(f+\Delta f, t+\Delta t)\right\}\mathrm{Re}\left\{P_1^y(f,t)\right\}\right] \\ &= \frac{1}{2}\mathrm{Re}\left\{C_{P_2^yP_1^y}(\Delta f, \Delta t, L_z, L_y)\right\}, \end{aligned} \tag{17}$$

where $C_{P_2^zP_1^z}(\Delta f, \Delta t, L_z, L_y)$ and $C_{P_2^yP_1^y}(\Delta f, \Delta t, L_z, L_y)$ are given as Eqs. (8) and (9), respectively.

IV. ZCRS OF PARTICLE VELOCITY CHANNELS

Let $\alpha(t)$ be a real random process with the temporal autocorrelation $\Gamma_\alpha(\Delta t) = E[\alpha(t+\Delta t)\ \alpha(t)]$. Then the ZCR of $\alpha(t)$, the average number of times that $\alpha(t)$ crosses the threshold zero per unit time, can be calculated using the following formula:[35,36]

$$n_\alpha^t = \frac{1}{\pi}\sqrt{\frac{-\Gamma_\alpha''(\Delta t)\big|_{\Delta t=0}}{\Gamma_\alpha(0)}}, \tag{18}$$

where double prime is the second derivative. Similarly, if $\alpha(f)$ is a real random process in the frequency domain, then its ZCR, n_α^f, the average number of times that $\alpha(f)$ crosses the threshold zero per unit frequency, is given by

$$n_\alpha^f = \frac{1}{\pi}\sqrt{\frac{-\Gamma_\alpha''(\Delta f)\big|_{\Delta f=0}}{\Gamma_\alpha(0)}}, \tag{19}$$

where $\Gamma_\alpha(\Delta f) = E[\alpha(f+\Delta f)\ \alpha(f)]$ is the frequency autocorrelation of $\alpha(f)$.

To study the delay and Doppler spreads of particle velocity channels, we need to calculate frequency- and time-domain ZCRs of the real parts of the complex channels $P^z(f, t)$ and $P^y(f, t)$. To do this, first the autocorrelation of the real part of the pressure channel, $\mathrm{Re}\{P(f,t)\}$, should be determined. Using Eqs. (5) and (11) we have

$$\begin{aligned} \Gamma_{\mathrm{Re}\{P\}}(\Delta f, \Delta t) &= E[\mathrm{Re}\{P(f+\Delta f, t+\Delta t)\}\mathrm{Re}\{P(f,t)\}] \\ &= \frac{1}{2}\mathrm{Re}\{C_{PP}(\Delta f, \Delta t)\}. \end{aligned} \tag{20}$$

The autocorrelation of the real part of the vertical particle velocity channel, $\mathrm{Re}\{P^z(f, t)\}$, can be written using Eqs. (12) and (16),

$$\begin{aligned} \Gamma_{\mathrm{Re}\{P^z\}}(\Delta f, \Delta t) &= E[\mathrm{Re}\{P^z(f+\Delta f, t+\Delta t)\}\mathrm{Re}\{P^z(f,t)\}] \\ &= \frac{1}{2}\mathrm{Re}\{C_{P^zP^z}(\Delta f, \Delta t)\}. \end{aligned} \tag{21}$$

Similarly, based on Eqs. (13) and (17), the autocorrelation of the real part of the horizontal velocity channel, $\mathrm{Re}\{P^y(f, t)\}$, is given by

$$\begin{aligned} \Gamma_{\mathrm{Re}\{P^y\}}(\Delta f, \Delta t) &= E[\mathrm{Re}\{P^y(f+\Delta f, t+\Delta t)\}\mathrm{Re}\{P^y(f,t)\}] \\ &= \frac{1}{2}\mathrm{Re}\{C_{P^yP^y}(\Delta f, \Delta t)\}. \end{aligned} \tag{22}$$

A. Frequency-domain ZCRs

Here we have $\Delta t = 0$. By inserting Eq. (11) into (20), taking derivative with respect to Δf twice and then replacing Δf with zero, for the pressure channel we obtain,

$$-\Gamma''_{\mathrm{Re}\{P\}}(\Delta f, 0)\Big|_{\Delta f=0} = \frac{\Lambda_b (2\pi T_b)^2}{2} E_{\gamma^b}\left[\frac{1}{\sin^2(\gamma^b)}\right] + \frac{(1-\Lambda_b)(2\pi T_s)^2}{2} E_{\gamma^s}\left[\frac{1}{\sin^2(\gamma^s)}\right]. \tag{23}$$

Note that $E_{\gamma^b}[\cdot]$ and $E_{\gamma^s}[\cdot]$ are expected values with respect to γ^b and γ^s, respectively. Similarly, by inserting Eq. (12) into (21) [or Eq. (13) into (22)], differentiation with respect to Δf twice and then replacing Δf with zero, for the vertical (or the horizontal) velocity channel we obtain,

$$-\Gamma''_{\mathrm{Re}\{P^z\}}(\Delta f, 0)\Big|_{\Delta f=0} = \frac{\Lambda_b (2\pi T_b)^2}{2} + \frac{(1-\Lambda_b)(2\pi T_s)^2}{2}, \tag{24}$$

$$-\Gamma''_{\mathrm{Re}\{P^y\}}(\Delta f, 0)\Big|_{\Delta f=0} = \frac{\Lambda_b (2\pi T_b)^2}{2} E_{\gamma^b}\left[\frac{\cos^2(\gamma^b)}{\sin^2(\gamma^b)}\right] + \frac{(1-\Lambda_b)(2\pi T_s)^2}{2} E_{\gamma^s}\left[\frac{\cos^2(\gamma^s)}{\sin^2(\gamma^s)}\right]. \tag{25}$$

Moreover, by inserting Eqs. (11)–(13) into Eqs. (20)–(22), respectively, it is easy to verify,

$$\Gamma_{\mathrm{Re}\{P\}}(0,0) = \frac{1}{2}, \tag{26}$$

$$\Gamma_{\mathrm{Re}\{P^z\}}(0,0) = \frac{\Lambda_b}{2} E_{\gamma^b}\left[\sin^2(\gamma^b)\right] + \frac{(1-\Lambda_b)}{2} E_{\gamma^s}\left[\sin^2(\gamma^s)\right], \tag{27}$$

$$\Gamma_{\mathrm{Re}\{P^y\}}(0,0) = \frac{\Lambda_b}{2} E_{\gamma^b}\left[\cos^2(\gamma^b)\right] + \frac{(1-\Lambda_b)}{2} E_{\gamma^s}\left[\cos^2(\gamma^s)\right]. \tag{28}$$

To obtain $n^f_{\mathrm{Re}\{P\}}$, $n^f_{\mathrm{Re}\{P^z\}}$, and $n^f_{\mathrm{Re}\{P^y\}}$, frequency-domain ZCRs, one needs to simply divide Eqs. (23)–(25) by Eqs. (26)–(28), respectively.

B. Time-domain ZCRs

Now we have $\Delta f = 0$. Similarly to the previous frequency-domain derivations, we can obtain the following results in time domain,

$$-\Gamma''_{\mathrm{Re}\{P\}}(0, \Delta t)\Big|_{\Delta t=0} = \frac{\Lambda_b (2\pi f_M)^2}{2} E_{\gamma^b}\left[\cos^2(\gamma^b - \varphi)\right] + \frac{(1-\Lambda_b)(2\pi f_M)^2}{2} E_{\gamma^s} \times \left[\cos^2(\gamma^s - \varphi)\right], \tag{29}$$

$$-\Gamma''_{\mathrm{Re}\{P^z\}}(0, \Delta t)\Big|_{\Delta t=0} = \frac{\Lambda_b (2\pi f_M)^2}{2} \times E_{\gamma^b}\left[\sin^2(\gamma^b)\cos^2(\gamma^b - \varphi)\right] + \frac{(1-\Lambda_b)(2\pi f_M)^2}{2} \times E_{\gamma^s}\left[\sin^2(\gamma^s)\cos^2(\gamma^s - \varphi)\right], \tag{30}$$

$$-\Gamma''_{\mathrm{Re}\{P^y\}}(0, \Delta t)\Big|_{\Delta t=0} = \frac{\Lambda_b (2\pi f_M)^2}{2} \times E_{\gamma^b}\left[\cos^2(\gamma^b)\cos^2(\gamma^b - \varphi)\right] + \frac{(1-\Lambda_b)(2\pi f_M)^2}{2} \times E_{\gamma^s}\left[\cos^2(\gamma^s)\cos^2(\gamma^s - \varphi)\right]. \tag{31}$$

By dividing Eqs. (29)–(31) by Eqs. (26)–(28), respectively, time-domain ZCRs $n^t_{\mathrm{Re}\{P\}}$, $n^t_{\mathrm{Re}\{P^z\}}$, and $n^t_{\mathrm{Re}\{P^y\}}$ will be obtained.

Note that the concept of channel ZCR is not limited to a certain frequency range. As long as channel correlation functions are available, one can calculate channel ZCRs, as explained in this section. To represent channels and calculate their correlation functions, however, we have used a ray-based framework. So, the derived results are appropriate for frequencies where ray analysis is relevant, say, high frequencies.

V. A CASE STUDY

Equations (23)–(31), which determine ZCR and therefore delay and Doppler spreads, are valid for any AOA distribution model. Here we use the Gaussian model,[31,37]

$$w^b(\gamma^b) = (2\pi\sigma_b^2)^{-1/2} \exp[-(\gamma^b - \mu_b)^2 \big/ (2\sigma_b^2)], \gamma^b \in (0, \pi),$$
$$w^s(\gamma^s) = (2\pi\sigma_s^2)^{-1/2} \exp[-(\gamma^s - \mu_s)^2 \big/ (2\sigma_s^2)], \gamma^s \in (\pi, 2\pi). \tag{32}$$

Note that μ_b and μ_s are the mean AOAs from the bottom and surface, respectively, whereas σ_b and σ_s represent angle spreads. Gaussian PDFs in Eq. (32) are particularly useful when angle spreads are small.[38] Based on experimental data, Gaussian PDFs with small variances are observed to be suitable for statistical modeling of an underwater acoustic channel.[37] For large angle spreads, one can use the von Mises PDF.[39]

For Gaussian AOA PDFs with small angle spreads, mathematical expectations in Eqs. (23)–(31) can be calculated in closed-forms, using the Taylor series expansions of γ^b and γ^s around μ_b and μ_s, respectively. For example,

$$\frac{1}{\sin^2(\gamma^b)} \approx \csc^2(\mu_b) - 2\csc^2(\mu_b)\cot(\mu_b)(\gamma^b - \mu_b) + (\cos(2\mu_b) + 2)\csc^4(\mu_b)(\gamma^b - \mu_b)^2, \tag{33}$$

where $\csc(\cdot)=1/\sin(\cdot)$ and $\cot(\cdot)=\cos(\cdot)/\sin(\cdot)$. Since $E_{\gamma^b}[\gamma^b-\mu_b]=0$ and $E_{\gamma^b}[(\gamma^b-\mu_b)^2]=\sigma_b^2$, Eq. (33) simplifies to

$$E_{\gamma^b}\left[\frac{1}{\sin^2(\gamma^b)}\right] \approx \csc^2(\mu_b) + (\cos(2\mu_b)+2)\csc^4(\mu_b)\sigma_b^2 \tag{34}$$

Following the same approach, one can calculate other $E_{\gamma^b}[\cdot]$ in Eqs. (25)–(31) as

$$E_{\gamma^b}\left[\frac{\cos^2(\gamma^b)}{\sin^2(\gamma^b)}\right] \approx \cot^2(\mu_b) + (\cos(2\mu_b)+2)\csc^4(\mu_b)\sigma_b^2, \tag{35}$$

$$E_{\gamma^b}\left[\sin^2(\gamma^b)\right] \approx \sin^2(\mu_b) + \cos(2\mu_b)\sigma_b^2, \tag{36}$$

$$E_{\gamma^b}\left[\cos^2(\gamma^b)\right] \approx \cos^2(\mu_b) - \cos(2\mu_b)\sigma_b^2, \tag{37}$$

$$E_{\gamma^b}\left[\cos^2(\gamma^b-\varphi)\right] \approx \cos^2(\mu_b-\varphi) + \cos(2\mu_b-2\varphi)\sigma_b^2, \tag{38}$$

$$\begin{aligned} &E_{\gamma^b}\left[\sin^2(\gamma^b)\cos^2(\gamma^b-\varphi)\right] \\ &\approx \cos^2(\mu_b-\varphi)\sin^2(\mu_b) + 0.5(\cos(2\mu_b) \\ &\quad +2\cos(4\mu_b-2\varphi) - \cos(2\mu_b-2\varphi))\sigma_b^2, \end{aligned} \tag{39}$$

$$\begin{aligned} &E_{\gamma^b}\left[\cos^2(\gamma^b)\cos^2(\gamma^b-\varphi)\right] \\ &\approx \cos^2(\mu_b)\cos^2(\mu_b-\varphi) - 0.5(\cos(2\mu_b) \\ &\quad +2\cos(4\mu_b-2\varphi) + \cos(2\mu_b-2\varphi))\sigma_b^2. \end{aligned} \tag{40}$$

Clearly, similar results can be obtained for γ^s, in terms of μ_s and σ_s.

To obtain some insight, we consider a case where the bottom components are dominant, i.e., $\Lambda_b=1$. Then we provide closed-form frequency- and time-domain ZCRs in the following subsections.

A. Frequency-domain ZCRs

By inserting Eqs. (23)–(28) into the ZCR formula in Eq. (19) and using the small angle spread approximation in Eqs. (34)–(37), one can show that

$$n^f_{\mathrm{Re}\{P\}} = 2T_b\left[\csc^2(\mu_b) + (\cos(2\mu_b)+2)\csc^4(\mu_b)\sigma_b^2\right]^{1/2}, \tag{41}$$

$$n^f_{\mathrm{Re}\{P^z\}} = 2T_b\left[\frac{1}{\sin^2(\mu_b)+\cos(2\mu_b)\sigma_b^2}\right]^{1/2}, \tag{42}$$

$$n^f_{\mathrm{Re}\{P^y\}} = 2T_b\left[\frac{\cot^2(\mu_b) + (\cos(2\mu_b)+2)\csc^4(\mu_b)\sigma_b^2}{\cos^2(\mu_b)-\cos(2\mu_b)\sigma_b^2}\right]^{1/2}. \tag{43}$$

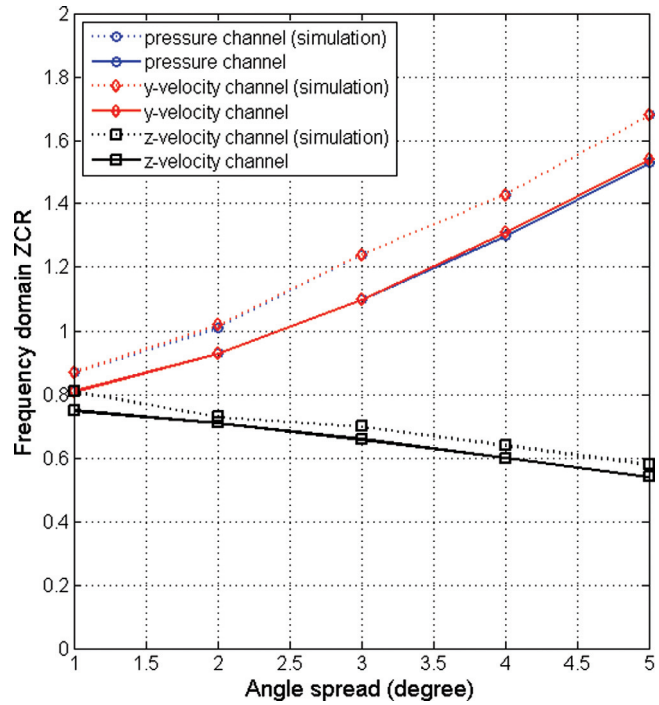

FIG. 4. (Color online) Frequency-domain ZCRs of particle velocity and pressure channels versus the angle spread $\sigma_b(\mu_b=5°)$.

Equations (41)–(43), normalized by T_b, are plotted in Fig. 4. Simulation results are also included, which show the accuracy of derived formulas. In simulations, the depth of the shallow water channel is 100 m. Center frequency is 12 kHz, sound speed is considered to be 1500 m/s, number of received rays is 50, and the speed of the vector sensor receiver initially located at a 50 m depth is 2.5 m/s.

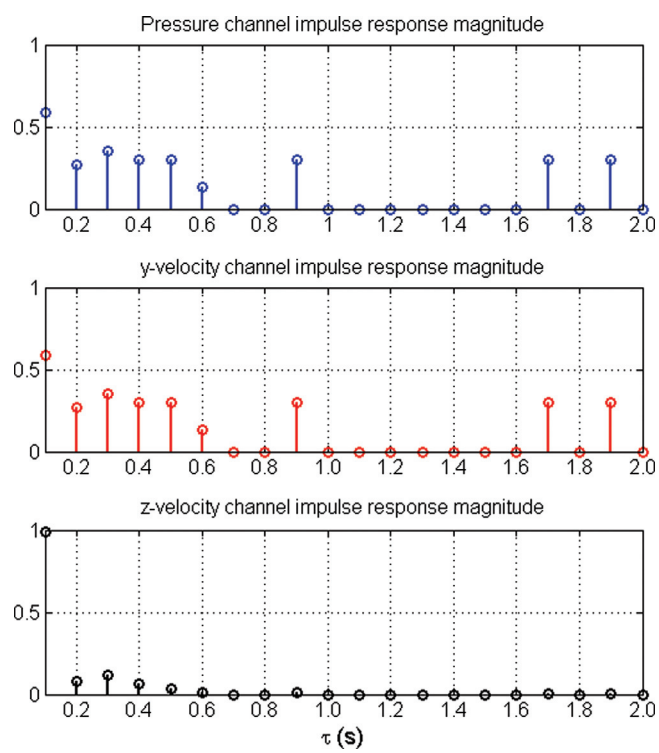

FIG. 5. (Color online) Normalized impulse responses of particle velocity channel and pressure channel.

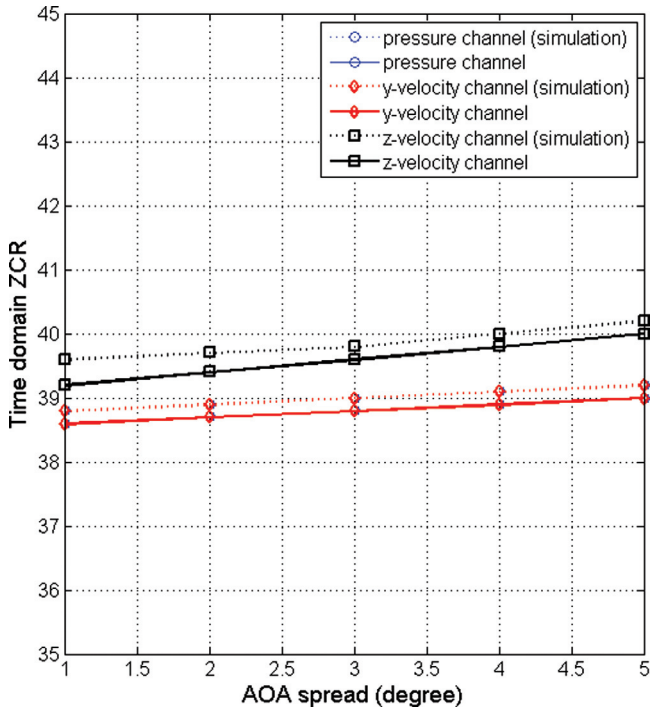

FIG. 6. (Color online) Time-domain ZCRs of particle velocity and pressure channels versus the angle spread $\sigma_b(\mu_b = 5°, \varphi = 0°)$.

Figure 4 shows the dependence of frequency-domain ZCRs on the angle spread. As expected, the ZCRs of y-velocity and pressure channels are very close. This is because the waves are coming through an almost horizontal direction ($\mu_b = 5°$). Increase of ZCRs with the angle spread can be related to the fact that as the angle spread increases, more rays from different directions reach the receiver. This means larger delay spreads, which results in large ZCRs in the frequency domain. Since in the case considered in Fig. 4, most of the AOAs are horizontal, the coming rays do not contribute much to the z-velocity channel. This explains the lower values of the frequency-domain z-velocity ZCR. This can be better understood by comparing the impulse responses of particle velocity and pressure channels in Fig. 5. This figure is obtained by plotting the impulse response in Eq. (6)[31] and its derivatives with respect to y and z, for $\mu_b = 5°$ and $\sigma_b = 3°$. Clearly the impulse response of the z channel is spread over a small range of delays in this example. These are consistent with other delay spread results,[34] obtained via a different approach. The advantage of the proposed velocity channel delay spread analysis here via frequency-domain ZCR is that it provides analytical expressions such as Eqs. (42) and (43). These types of expressions quantify the delay spreads of acoustic particle velocity and pressure channels in terms of key channel parameters such as mean AOAs and angle spreads. Further results are provided in Appendix B, which shed some light on the behavior of delay spread in particle velocity channels.

B. Time-domain ZCRs

By inserting Eqs. (29)–(31) and Eqs. (26)–(28) into the ZCR formula in Eq. (18) and using the small angle spread approximation in Eqs. (36)–(40), the following results can be obtained.

$$n^t_{\mathrm{Re}\{P\}} = 2f_M\left[\cos^2(\mu_b - \varphi) + \cos(2\mu_b - 2\varphi)\sigma_b^2\right]^{1/2}, \tag{44}$$

$$n^t_{\mathrm{Re}\{P^z\}} = 2f_M\left[\frac{\cos^2(\mu_b - \varphi)\sin^2(\mu_b) + \frac{1}{2}(\cos(2\mu_b) + 2\cos(4\mu_b - 2\varphi) - \cos(2\mu_b - 2\varphi))\sigma_b^2}{\sin^2(\mu_b) + \cos(2\mu_b)\sigma_b^2}\right]^{1/2}, \tag{45}$$

$$n^t_{\mathrm{Re}\{P^y\}} = 2f_M\left[\frac{\cos^2(\mu_b)\cos^2(\mu_b - \varphi) - \frac{1}{2}(\cos(2\mu_b) + 2\cos(4\mu_b - 2\varphi) + \cos(2\mu_b - 2\varphi))\sigma_b^2}{\cos^2(\mu_b) - \cos(2\mu_b)\sigma_b^2}\right]^{1/2}. \tag{46}$$

Equations (44)–(46), normalized by f_M are plotted in Fig. 6, along with simulation results, which demonstrate the accuracy of the analytical results. According to this figure, time-domain ZCRs of particle velocity and pressure channels are about the same and not dependent much on the angle spread, for the case considered. The analysis conducted in Appendix B for other conditions provides more insight on Doppler spread in these communication channels.

VI. CONCLUSION

In this paper, a zero-crossing framework is developed to study the delay and Doppler spreads in multipath underwater acoustic particle velocity and pressure channels. A geometrical–statistical representation of the shallow water waveguide is considered, to derive the required frequency- and time-domain channel correlation functions. Then the delay and Doppler spreads are calculated by deriving closed-form expressions for the channel ZCRs in frequency and time, respectively. These expressions show how velocity channel delay and Doppler spreads may depend on some key parameters of the channel such as mean AOA and angle spread. The results are useful for design and performance prediction of vector sensor systems that operate in acoustic particle velocity channels.

ACKNOWLEDGMENTS

This work is supported in part by the National Science Foundation (NSF), Grant CCF-0830190.

APPENDIX A: PARAMETERS OF THE PRESSURE CHANNEL CORRELATION FUNCTION

Here we show how all the parameter and variables in the pressure channel correlation function in Eq. (5) can be expressed in terms of γ^b and γ^s, the bottom and surface AOAs, respectively, and also L_z, L_y, D, and D_0. According to Fig. 3, it is straightforward to verify,

$$\sin(\gamma_1^b) = (D_0 - D + (L_z/2))/\xi_1^b,$$
$$\sin(\gamma_2^b) = (D_0 - D - (L_z/2))/\xi_2^b, \tag{A1}$$

$$\sin(\gamma_1^s) = -(D - (L_z/2))/\xi_1^s,$$
$$\sin(\gamma_2^s) = -(D + (L_z/2))/\xi_2^s, \tag{A2}$$

$$\cos(\gamma_1^b) = [(D_0 - D)\cot(\gamma^b) - (L_y/2)]/\xi_1^b,$$
$$\cos(\gamma_2^b) = [(D_0 - D)\cot(\gamma^b) + (L_y/2)]/\xi_2^b, \tag{A3}$$

$$\cos(\gamma_1^s) = -[D\cot(\gamma^s) + (L_y/2)]/\xi_1^s,$$
$$\cos(\gamma_2^s) = -[D\cot(\gamma^s) - (L_y/2)]/\xi_2^s, \tag{A4}$$

where $\cot(\cdot) = \cos(\cdot)/\sin(\cdot)$. Moreover, ξ_1^b, ξ_2^b, ξ_1^s, and ξ_2^s are rays travel distances from the sea bottom and surface to Rx_1 and Rx_2, respectively, and can be expressed as

$$\xi_1^b = \sqrt{(D_0 - D)^2 + L^2\sin^2(\gamma^b) - 2(D_0 - D)L\cos\left(\frac{\pi}{2} + \gamma^b - \arctan\left(\frac{L_y}{L_z}\right)\right)\sin(\gamma^b)}\Big/\sin(\gamma^b), \tag{A5}$$

$$\xi_2^b = \sqrt{(D_0 - D)^2 + L^2\sin^2(\gamma^b) - 2(D_0 - D)L\cos\left(\frac{\pi}{2} - \gamma^b + \arctan\left(\frac{L_y}{L_z}\right)\right)\sin(\gamma^b)}\Big/\sin(\gamma^b), \tag{A6}$$

$$\xi_1^s = -\sqrt{D^2 + L^2\sin^2(\gamma^s) - 2DL\cos\left(\frac{\pi}{2} + \gamma^s - \arctan\left(\frac{L_y}{L_z}\right)\right)\sin(\gamma^s)}\Big/\sin(\gamma^s), \tag{A7}$$

$$\xi_2^s = -\sqrt{D^2 + L^2\sin^2(\gamma^s) - 2DL\cos\left(\frac{\pi}{2} - \gamma^s + \arctan\left(\frac{L_y}{L_z}\right)\right)\sin(\gamma^s)}\Big/\sin(\gamma^s). \tag{A8}$$

Moreover, τ_q^b and τ_q^s in Eq. (5), $q = 1, 2$, are the travel times from bottom and surface scatterers to the Rx_1 and Rx_2, respectively, which are given by

$$\tau_1^b = \frac{\xi_1^b}{c}, \quad \tau_2^b = \frac{\xi_2^b}{c}, \quad \tau_1^s = \frac{\xi_1^s}{c}, \quad \tau_2^s = \frac{\xi_2^s}{c}, \tag{A9}$$

where c is the sound speed.

By inserting Eqs. (A1)–(A9) into Eq. (5), one obtains the pressure channel frequency-time-space correlation as two integrals over the bottom and surface AOAs γ^b and γ^s, respectively. For any given AOA PDFs $w^b(\gamma^b)$ and $w^s(\gamma^s)$, the two integrals in Eq. (5) can be computed numerically. For some special cases of interest such as vertical and horizontal vector sensor arrays discussed below, Eqs. (A1)–(A8) can be significantly simplified. This allows to calculate the integrals in Eq. (5) analytically.[34]

A. Vertical vector sensor array

For $L_z \ll \min(D, D_0 - D)$, $L_y = 0$ and using $\sqrt{1+x} \approx 1 + (x/2)$ when $|x| \ll 1$, distances ξ_1^b, ξ_2^b, ξ_1^s, and ξ_2^s given in Eqs. (A5)–(A8) can be approximated as

$$\xi_1^b \approx [(D_0 - D) + L_z\sin^2(\gamma^b)/2]/\sin(\gamma^b),$$
$$\xi_2^b \approx [(D_0 - D) - L_z\sin^2(\gamma^b)/2]/\sin(\gamma^b),$$
$$\xi_1^s \approx -[D - (L_z\sin^2(\gamma^s)/2)]/\sin(\gamma^s),$$
$$\xi_2^s \approx -[D + (L_z\sin^2(\gamma^s)/2)]/\sin(\gamma^s). \tag{A10}$$

Then substitution of Eq. (A10) into Eqs. (A1)–(A4) and (A9), results in

$$\sin(\gamma_2^b) - \sin(\gamma_1^b) \approx L_z\sin^3(\gamma^b)/(D_0 - D),$$
$$\sin(\gamma_2^s) - \sin(\gamma_1^s) \approx -L_z\sin^3(\gamma^s)/D, \tag{A11}$$

$$\sin(\gamma_2^b) + \sin(\gamma_1^b) \approx 2\sin(\gamma^b),$$
$$\sin(\gamma_2^s) + \sin(\gamma_1^s) \approx 2\sin(\gamma^s), \tag{A12}$$

$$\tau_1^b - \tau_2^b \approx L_z\sin(\gamma^b)/c,$$
$$\tau_1^s - \tau_2^s \approx L_z\sin(\gamma^s)/c, \tag{A13}$$

$$\tau_2^b \approx (D_0 - D)/(c\sin(\gamma^b)),$$
$$\tau_2^s \approx -D/(c\sin(\gamma^s)). \tag{A14}$$

B. Horizontal vector sensor array

Similarly, when $L_y \ll \min(D, D_0 - D)$ and $L_z = 0$, the distances ξ_1^b, ξ_2^b, ξ_1^s, and ξ_2^s given in Eqs. (A5)–(A8) can be similarly approximated by

$$\begin{aligned}
\xi_1^b &\approx [(D_0 - D) - (L_y \sin(\gamma^b)\cos(\gamma^b))/2]/\sin(\gamma^b),\\
\xi_2^b &\approx [(D_0 - D) + (L_y \sin(\gamma^b)\cos(\gamma^b))/2]/\sin(\gamma^b),\\
\xi_1^s &\approx -[D + (L_y \sin(\gamma^s)\cos(\gamma^s))/2]/\sin(\gamma^s),\\
\xi_2^s &\approx -[D - (L_y \sin(\gamma^s)\cos(\gamma^s))/2]/\sin(\gamma^s).
\end{aligned} \tag{A15}$$

Substitution of Eq. (A5) into Eqs. (A1)–(A4) results in

$$\begin{aligned}
\sin(\gamma_2^b) - \sin(\gamma_1^b) &\approx -\frac{L_y}{D_0 - D}\left(\frac{\cos(\gamma^b) - \cos(3\gamma^b)}{4}\right),\\
\sin(\gamma_2^s) - \sin(\gamma_1^s) &\approx \frac{L_y}{D}\left(\frac{\cos(\gamma^s) - \cos(3\gamma^s)}{4}\right),
\end{aligned} \tag{A16}$$

$$\begin{aligned}
\cos(\gamma_2^b) + \cos(\gamma_1^b) &\approx 2\cos(\gamma^b),\\
\cos(\gamma_2^s) + \cos(\gamma_1^s) &\approx 2\cos(\gamma^s),
\end{aligned} \tag{A17}$$

$$\begin{aligned}
\tau_1^b - \tau_2^b &\approx -L_y \cos(\gamma^b)/c,\\
\tau_1^s - \tau_2^s &\approx -L_y \cos(\gamma^s)/c,
\end{aligned} \tag{A18}$$

$$\begin{aligned}
\tau_2^b &\approx (D_0 - D)/(c\sin(\gamma^b)),\\
\tau_2^s &\approx -D/(c\sin(\gamma^s)).
\end{aligned} \tag{A19}$$

Using Eqs. (A10)–(A19) and for Gaussian AOA PDFs with small angle spreads, on can solve the integrals in Eq. (5) in closed forms.[34] Differentiation with respect to L_z or L_y provides integral-free expressions for z- and y-particle velocity channels, respectively.

APPENDIX B: COMPARISON OF VELOCITY CHANNEL ZCRS

To better understand delay and Doppler spreads of acoustic particle velocity channels, here we consider the practical case where most of the rays in shallow water come along the horizontal direction. This implies that mean AOAs are relatively small, which enable us to further analyze velocity channel ZCRs. Similarly to Sec. V, we consider the case where the bottom rays are dominant. With pressure channel ZCR as a reference, in what follows we compare the ZCRs of particle velocity channels.

A. Frequency-domain ZCRs

Without less of generality and to simplify the notation, we consider the square root value of ZCRs. Using Eqs. (41)–(43), the frequency-domain ZCRs of velocity channels with respect to the pressure channel can be written as

$$\left(\frac{n^f_{\mathrm{Re}\{P^z\}}}{n^f_{\mathrm{Re}\{P\}}}\right)^2 = \frac{1/[\sin^2(\mu_b) + \cos(2\mu_b)\sigma_b^2]}{\csc^2(\mu_b) + (\cos(2\mu_b) + 2)\csc^4(\mu_b)\sigma_b^2}, \tag{B1}$$

$$\left(\frac{n^f_{\mathrm{Re}\{P^y\}}}{n^f_{\mathrm{Re}\{P\}}}\right)^2 = \frac{[\cot^2(\mu_b) + (\cos(2\mu_b) + 2)\csc^4(\mu_b)\sigma_b^2/\cos^2(\mu_b) - \cos(2\mu_b)\sigma_b^2]}{\csc^2(\mu_b) + (\cos(2\mu_b) + 2)\csc^4(\mu_b)\sigma_b^2}. \tag{B2}$$

Using the first-order Taylor series expansions $\sin(\mu_b) \approx \mu_b$, and $\cos(\mu_b)$, $\cos(2\mu_b) \approx 1$, when μ_b is small, it is straightforward to verify,

$$\left(\frac{n^f_{\mathrm{Re}\{P^z\}}}{n^f_{\mathrm{Re}\{P\}}}\right)^2 \approx \frac{1}{1 + 4(\sigma_b/\mu_b)^2 + 3(\sigma_b/\mu_b)^4}, \tag{B3}$$

$$\left(\frac{n^f_{\mathrm{Re}\{P^y\}}}{n^f_{\mathrm{Re}\{P\}}}\right)^2 \approx \frac{1}{1 - \sigma_b^2}. \tag{B4}$$

According to Eq. (B3), ZCR of the z-velocity channel can be smaller than the pressure channel, whereas Eq. (B4) shows the ZCRs of the y-velocity channel and pressure channels are nearly the same. These are consistent with the observations made in Sec. V.

B. Time-domain ZCRs

Based on Eqs. (44)–(46), time-domain ZCRs of z- and y-velocity channels with respect to the pressure channel are given as

$$\left(\frac{n^t_{\mathrm{Re}\{P^z\}}}{n^t_{\mathrm{Re}\{P\}}}\right)^2 = \frac{\cos^2(\mu_b - \varphi)\sin^2(\mu_b) + 0.5(\cos(2\mu_b) + 2\cos(4\mu_b - 2\varphi) - \cos(2\mu_b - 2\varphi))\sigma_b^2}{(\cos^2(\mu_b - \varphi) + \cos(2\mu_b - 2\varphi)\sigma_b^2)(\sin^2(\mu_b) + \cos(2\mu_b)\sigma_b^2)}, \tag{B5}$$

$$\left(\frac{n^t_{\mathrm{Re}\{P^y\}}}{n^t_{\mathrm{Re}\{P\}}}\right)^2 = \frac{\cos^2(\mu_b)\cos^2(\mu_b - \varphi) - 0.5(\cos(2\mu_b) + 2\cos(4\mu_b - 2\varphi) + \cos(2\mu_b - 2\varphi))\sigma_b^2}{(\cos^2(\mu_b - \varphi) + \cos(2\mu_b - 2\varphi)\sigma_b^2)(\cos^2(\mu_b) - \cos(2\mu_b)\sigma_b^2)}. \tag{B6}$$

For $\varphi = 0$ and using the first order Taylor series mentioned previously, Eqs. (B5) and (B6) can be simplified to

$$\left(\frac{n^t_{\mathrm{Re}\{P^z\}}}{n^t_{\mathrm{Re}\{P\}}}\right)^2 \approx \frac{1}{1+\sigma_b^2}, \tag{B7}$$

$$\left(\frac{n^t_{\mathrm{Re}\{P^y\}}}{n^t_{\mathrm{Re}\{P\}}}\right)^2 \approx 1 - 2\sigma_b^2. \tag{B8}$$

On the other hand, $\varphi = \pi/2$ simplifies Eqs. (B5) and (B6) to

$$\left(\frac{n^t_{\mathrm{Re}\{P^z\}}}{n^t_{\mathrm{Re}\{P\}}}\right)^2 \approx \frac{1}{1-(\sigma_b/\mu_b)^4}, \tag{B9}$$

$$\left(\frac{n^t_{\mathrm{Re}\{P^y\}}}{n^t_{\mathrm{Re}\{P\}}}\right)^2 \approx \frac{1+(\sigma_b/\mu_b)^2}{1-(\sigma_b/\mu_b)^2}. \tag{B10}$$

Here we observe that when the receiver moves horizontally toward the transmitter, ZCRs of z- and y-velocity channels are almost the same as the pressure channel ZCR, according to Eqs. (B7) and (B8). When the receiver moves vertically toward the bottom, there ratios could be somewhat different. Given the shallow depth of the channel, this holds only over a short period of time.

[1]D. B. Kilfoyle and A. B. Baggeroer, "The state of the art in underwater acoustic telemetry," IEEE J. Ocean. Eng. **25**, 4–27 (2000).

[2]M. Stojanovic, J. A. Catipovic, and J. G. Proakis, "Reduced-complexity spatial and temporal processing of underwater acoustic communication signals," J. Acoust. Soc. Am. **98**, 961–972 (1995).

[3]M. Stojanovic, J. A. Catipovic, and J. G. Proakis, "Phase-coherent digital communications for underwater acoustic channels," IEEE J. Ocean. Eng. **19**, 100–111 (1994).

[4]A. Song, M. Badiey, and V. K. McDonald, "Multichannel combining and equalization for underwater acoustic MIMO channels," in *Proceedings of Oceans*, Kobe, Japan (2008).

[5]S. Roy, T. M. Duman, V. McDonald, and J. G. Proakis, "High rate communication for underwater acoustic channels using multiple transmitters and space-time coding: Receiver structures and experimental results," IEEE J. Ocean. Eng. **32**, 663–688 (2007).

[6]H. C. Song, W. S. Hodgkiss, W. A. Kuperman, W. J. Higley, K. Raghukumar, and T. Akal, "Spatial diversity in passive time reversal communications," J. Acoust. Soc. Am. **120**, 2067–2076 (2006).

[7]D. B. Kilfoyle, J. C. Preisig, and A. B. Baggeroer, "Spatial modulation experiments in the underwater acoustic channel," IEEE J. Ocean. Eng. **30**, 406–415 (2005).

[8]H. F. Olson, "Mass controlled electrodynamic microphones: The ribbon microphone," J. Acoust. Soc. Am. **3**, 56–68 (1931).

[9]A. Nehorai and E. Paldi, "Acoustic vector-sensor array processing," IEEE Trans. Signal Process. **42**, 2481–2491 (1994).

[10]B. A. Cray and A. H. Nuttall, "Directivity factors for linear arrays of velocity sensors," J. Acoust. Soc. Am. **110**, 324–331 (2001).

[11]B. A. Cray, V. M. Evora, and A. H. Nuttall, "Highly directional acoustic receivers," J. Acoust. Soc. Am. **113**, 1526–1532 (2003).

[12]G. L. D'Spain, J. C. Luby, G. R. Wilson, and R. A. Gramann, "Vector sensors and vector sensor line arrays: Comments on optimal array gain and detection," J. Acoust. Soc. Am. **120**, 171–185 (2006).

[13]A. Abdi and H. Guo, "A new compact multichannel receiver for underwater wireless communication networks," IEEE Trans. Wireless Commun. **8**, 3326–3329 (2009).

[14]A. Abdi, H. Guo, and P. Sutthiwan, "A new vector sensor receiver for underwater acoustic communication," in *Proceedings of Oceans*, Vancouver, BC, Canada (2007).

[15]H. Guo and A. Abdi, "Multiuser underwater communication with space-time block codes and acoustic vector sensors," in *Proceedings of Oceans*, Quebec City, QC, Canada (2008).

[16]A. Song, A. Abdi, M. Badiey, and P. Hursky, "Time reversal receivers for underwater acoustic communication using vector sensors," in *Proceedings of MTS/IEEE Oceans,* Quebec City, QC, Canada (2008).

[17]D. Tse and P. Viswanath, *Fundamentals Wireless Communication* (Cambridge, New York, 2005), pp. 16–32.

[18]R. McDonald, K. Commander, J. Stroud, J. Wilbur, and G. Deane, "Channel characterization for communications in very shallow water," J. Acoust. Soc. Am. **111**, 2407 (2002).

[19]A. Morozov, J. Preisig, and J. Papp, "Modal processing for acoustic communications in shallow water experiment," J. Acoust. Soc. Am. **124**, 177–181 (2008).

[20]D. Rouseff, "Coherent communications performance in environments with strong multi-pathing: Model/data comparison," J. Acoust. Soc. Am. **125**, 2580 (2009).

[21]J. Rice, P. Baxley, H. Bucker, R. Shockley, D. Green, J. Proakis, and J. Newton, "Doppler spread in an undersea acoustic transmission channel," J. Acoust. Soc. Am. **103**, 2782 (1998).

[22]N. Bom and B. W. Conoly, "Zero-crossing shift as a detection method," J. Acoust. Soc. Am. **47**, 1408–1411 (1970).

[23]R. C. Spindel and P. T. McElroy, "Level and zero crossings in volume reverberation signals," J. Acoust. Soc. Am. **53**, 1417–1426 (1973).

[24]J. E. Ehrenberg, "An approximate bivariate density function for orthogonal filtered Poisson processes with applications to volume reverberation problems," J. Acoust. Soc. Am. **59**, 374–380 (1976).

[25]D. M. Egle, "A stochastic model for transient acoustic emission signals," J. Acoust. Soc. Am. **65**, 1198–1203 (1979).

[26]M. Balaraman, S. Dusan, and J. L. Flanagan, "Supplementary features for improving phone recognition," J. Acoust. Soc. Am. **116**, 2479 (2004).

[27]K. Witrisal, "On estimating the RMS delay spread from the frequency-domain level crossing rate," IEEE Commun. Lett. **5**, 287–289 (2001).

[28]K. Witrisal, Y. Kim, and R. Prasad, "A new method to measure parameters of frequency-selective radio channels using power measurements," IEEE Trans. Commun. **49**, 1788–1800 (2001).

[29]H. Zhang and A. Abdi, "On the average crossing rates in selection diversity," IEEE Trans. Wireless Commun. **6**, 448–451 (2007).

[30]N. C. Beaulieu and X. Dong, "Level crossing rate and average fade duration of MRC and EGC diversity in Ricean fading," IEEE Trans. Commun. **51**, 722–726 (2003).

[31]A. Abdi and H. Guo, "Signal correlation modeling in acoustic vector sensor arrays," IEEE Trans. Signal Process. **57**, 892–903 (2009).

[32]A. Abdi and M. Kaveh, "Parametric modeling and estimation of the spatial characteristics of a source with local scattering," in *Proceedings of IEEE International Conference on Acoustics, Speech, and Signal Processing*, Orlando, FL (2002), pp. 2821–2824.

[33]C. Bjerrum-Niese, L. Bjorno, M. A. Pinto, and B. Quellec, "A simulation tool for high data-rate acoustic communication in a shallow-water, time-varying channel," IEEE J. Ocean. Eng. **21**, 143–149 (1996).

[34]H. Guo, A. Abdi, A. Song, and M. Badiey, "Correlations in underwater acoustic particle velocity and pressure channels," in *Proceedings of Conference on Information Sciences and Systems*, Johns Hopkins University, Baltimore, MD (2009), pp. 913–918.

[35]A. Papoulis, *Probability, Rom Variables, Stochastic Processes*, 3rd ed. (Singapore, McGraw-Hill, 1991), pp. 513–521.

[36]G. L. Stuber, *Principles Mobile Communication* (Boston, MA, Kluwer, 1996), pp. 61–66.

[37]P. H. Dahl, "Observations and modeling of angular compression and vertical spatial coherence in sea surface forward scattering," J. Acoust. Soc. Am. **127**, 96–103 (2010).

[38]T. C. Yang, "A study of spatial processing gain in underwater acoustic communications," IEEE J. Ocean. Eng. **32**, 689–709 (2007).

[39]A. Abdi, J. A. Barger, and M. Kaveh, "A parametric model for the distribution of the angle of arrival and the associated correlation function and power spectrum at the mobile station," IEEE Trans. Veh. Technol. **51**, 425–434 (2002).